

Characterization of Flow Oblique to a Circular Cylinder with Low Aspect Ratio Using 3-D Detached Eddy Simulation

DongHun Yeo ^{a,*}, Nicholas P. Jones ^b

^a*Engineering Laboratory, National Institute of Standards and Technology, Gaithersburg, MD 20899, USA*

^b*G.W.C. Whiting School of Engineering, The Johns Hopkins University, Baltimore, MD 21218, USA*

ABSTRACT

Large-amplitude vibrations of stay cables in cable-stayed bridges can threaten the safety and serviceability of the structures. Understanding of the excitation mechanism is necessary to mitigate such vibrations effectively and efficiently. Experimental research has investigated the mechanism of oscillation using flow oblique to a cylinder; however, since the aspect ratio of the cylinder is much lower than that of a real stay cable in bridges, the results might not reliably describe the real phenomenon. The aim of this study is 1) to provide better understanding of aspect ratio effects of a circular cylinder on aerodynamic characteristics of the cylinder oblique to flow associated with the large-amplitude cable vibrations and 2) to provide to experimentalists suggestions of a requisite aspect ratio and appropriate pressure-measuring positions of a cylinder for fully developed flow around the cylinder. To this end the current work applied three-dimensional detached eddy simulations (DES) to flow around a yawed and inclined cylinder to investigate the importance of the aspect ratio of the cylinder when flow oblique to the cylinder develops fully along its spanwise axis. The Reynolds number is 1.4×10^5 based on the incoming flow velocity and the diameter of the cylinder. Three aspect ratios ($L/D = 10, 20, \text{ and } 30$; L : a cylinder length; D : a cylinder diameter) and two numerical conditions (slip and periodic) on

* Corresponding author. Tel: 1-301-975-8103; fax. 1-301-869-6275.
E-mail address: donghun.yeo@nist.gov (DongHun Yeo)

spanwise boundaries were employed. Results showed that three-dimensional flow and the associated forces on a yawed and inclined cylinder are significantly influenced by the spanwise aspect ratios and spanwise boundary conditions. This study suggests that when a wind tunnel experiment investigates flow oblique to a very slender cylinder, such as attempting to model a stay cable, experimentalists should use a sufficiently high spanwise aspect ratio of the cylinder. For the case of the 30° yaw and 45° inclined cylinder, the requisite ratio would be approximately 60 or higher and appropriate pressure-measuring positions of a half to two-thirds of the cylinder length from its upper/upstream end in order to accurately model inherently three-dimensional characteristics of the flow.

Keywords: cable vibration; cable-stayed bridge; yawed and inclined circular cylinder; detached eddy simulation; spanwise wall boundary condition; spanwise aspect ratio; end effect.

1. INTRODUCTION

Large-amplitude vibrations of stay cables are a serious concern in the safety and serviceability of cable-stayed bridges. These vibrations often occur with rain (Hikami and Shiraishi, 1988), but rain is not necessary for them to occur (Matsumoto et al., 1998; Zuo and Jones, 2006). Importantly, the oscillating cables are under oblique wind (Phelan et al., 2006; Zuo and Jones, 2006). These observations suggest that these vibrations are fully three-dimensional in nature and cannot necessarily be fully characterized with a two-dimensional model.

Wind tunnel experiments have observed three-dimensional characteristics of the flow oblique to a prototype cable or a circular cylinder of a low aspect ratio. Tournier and Py (1978)

investigated instantaneous surface velocities near a yawed cylinder; their observations indicated the existence of rotating flow structures with axial velocities near the cylinder surface. Shirakashi et al. (1986) demonstrated the presence of flow moving parallel to the cylinder axis in the wake behind a yawed cylinder. Matsumoto et al. (1990) confirmed an intense secondary axial flow on the leeward surface of a yawed cylinder in flow visualization tests. These authors suggested that the axial flow prevented the interaction between the two separated shear layers, much as a splitter plate would. Kohama and Motegi (1994) also detected traveling flow structures in the three-dimensional boundary layer associated with a yawed cylinder.

Wind tunnel tests also have addressed effects of side walls on flow and the associated forces on an oblique cylinder. Ramberg (1983) showed that the effect of end conditions on three-dimensional flow field was significant for a yawed cylinder with an aspect ratio of $L/D = 100$. Matsumoto et al. (2005) observed that velocities of axial flows around a yawed cylinder were influenced by the treatment of ends (i.e., free end, end plates, and windows of side walls). Their subsequent study (Matsumoto et al., 2007) reported high fluctuation of the data for a yawed cylinder even when they extended the spanwise aspect ratio to $L/D = 24$. Larose et al. (2003) attempted to rule out end effects in tests of an inclined cylinder by attaching elliptical plates at its ends. However, their data on a cylinder with an aspect ratio of 33 also showed significant spatial deviations between measuring points. This implies that the flow might not fully develop along the cylinder length even with end plates and a relatively high aspect ratio.

Aspect ratios of stay cables in cable-stayed bridges usually range from hundreds to thousands (Zuo, 2005). In a laboratory, experiments cannot adequately model the real aspect ratio of the stay cables for two reasons: 1) lack of overall testing space, and 2) insufficient room inside a cylinder for measuring equipment. The use of end plates to rule out the end effects in

experiments is also questionable. The plates reduce the disturbance of flow that is associated with the blunt ends of a cylinder, but they also prevent flow from developing in the spanwise direction. This is potentially a critical flow because inherently three-dimensional flow along a cylinder axis is a principal feature of flow oblique to a cylinder (Yeo and Jones, 2008b). The fully developed flow in the spanwise direction generates multiple force peaks that move along the length of the cylinder; these force peaks can produce excitation of the cylinder at much lower frequency than classical Kármán vortex-induced forces. Therefore, flow oblique to a finite cylinder in a laboratory set-up is influenced not only by the relative angle between the cylinder axis and the flow direction, but also by the disturbance of flow due to end plates and side walls of the wind tunnel. When the spanwise aspect ratio is not sufficiently high, this “end effect” on the flow is particularly dominant around an oblique cylinder.

However, numerical simulations in three dimensions provide more flexibility in modeling the flow developing along the cylinder axis. They have implemented spanwise boundary conditions on the ends of an oblique cylinder of a relatively low aspect ratio and have predicted reliably and efficiently the flow around a cylinder of an infinitely high ratio. Kawamura and Hayashi (1994) simulated the flow around a yawed cylinder using slip and periodic boundary conditions on spanwise walls. Results showed that flow was significantly affected by the slip boundary, especially near the upstream end of the cylinder. The end effect of the slip boundary condition on flow field was confirmed by Matsuzaki et al. (1994). Their simulations showed that as a cylinder shortened and its yaw angle increased, the disturbance of flow due to the end effect became more significant. Lucor and Karniadakis (2003) used the periodic condition on spanwise boundaries to simulate flow around a yawed cylinder. They observed a traveling “braid” of forces along the cylinder axis, but did not provide a detailed explanation.

Yeo and Jones (2006, 2008b) investigated three-dimensional characteristics of fully developed flow oblique to a cylinder using periodic boundary conditions. Results showed that swirling flows developed alternately from both sides of the cylinder section and moved along the cylinder axis. As noted previously, these flows play a principal role in generating inherent characteristics of forces; a series of force peaks at spatial intervals moves along the cylinder. A subsequent study (Yeo and Jones, 2008a) showed that slip boundary conditions prevent flow from developing the inherent features along the cylinder length, but the development of forces along the finite lengths of the cylinder between the slip walls was not investigated.

The present study is an extension of these previous efforts to further investigate the characteristics of flow and the associated forces on a cylinder with a low aspect ratio. This computational study aims at 1) better understanding how the spanwise length of a cylinder oblique to flow affects flow development around the cylinder and 2) providing to wind tunnel experimentalists useful information on a requisite aspect ratio and appropriate pressure-measuring positions of a cylinder for tests of fully developed flow oblique to a very slender cylinder, such as wind around a stay cable. It employed both slip and periodic boundary conditions on spanwise walls, and different aspect ratios were considered ($L/D = 10, 20, \text{ and } 30$) in three-dimensional detached eddy simulations of flow oblique to a cylinder. Flow development and the flow-induced aerodynamics forces on cylinders of the various limited length were investigated in comparison to those of a cylinder of infinite length.

2. NUMERICAL SIMULATION

2.1 Spalart-Allmaras DES Approach

Detached eddy simulation (DES) is a hybrid method combining the strengths of Reynolds-averaged Navier Stokes equations (RANS) in both boundary layer and mildly separated flow regions and of large eddy simulation (LES) in the massively separated flow region (Spalart et al., 1997). In the region near the boundary of a structure (e.g., close to a wall) where the local grid dimension is larger than the flow turbulence length scale, the model treats the region in a RANS-like manner. In contrast, in the region where the local grid spacing is much smaller than the flow turbulence length scale (e.g., away from a wall), the region is solved in an LES-like manner. The Spalart-Allmaras DES turbulence model used in this study (Spalart et al., 1997) is a modification of the Spalart-Allmaras (S-A) RANS turbulence model (Spalart and Allmaras, 1992) and adjusts the turbulence length scale of the model by switching the mode between RANS and LES.

The turbulent viscosity governing equation of the S-A DES model is

$$\frac{D\tilde{\nu}}{Dt} = c_{b1}\tilde{S}\tilde{\nu} + \frac{1}{\sigma}\left\{\nabla\cdot[(\nu+\tilde{\nu})\nabla\tilde{\nu}] + c_{b2}(\nabla\tilde{\nu})^2\right\} - c_{w1}f_w\left[\frac{\tilde{\nu}}{\tilde{d}}\right]^2. \quad (1)$$

From the above equation the turbulent kinematic viscosity is determined by $\nu_T = \tilde{\nu}f_{v1}$ where a function f_{v1} is decided in the proximity of walls. Definitions of coefficients and functions used in the above equation can be found in the original papers (Spalart and Allmaras, 1992; Spalart et al., 1997). In the Eq. (1), the last term in the right-hand side is related to destruction of turbulent viscosity, which depends on the DES turbulence length scale \tilde{d} defined as:

$$\tilde{d} \equiv \min(d, C_{\text{DES}} \Delta) \quad (2)$$

where d is the distance to the closest wall, and Δ is the maximum grid spacing (i.e., $\max(\Delta x, \Delta y, \Delta z)$) in the three-dimensional structured grid cell, and C_{DES} is the adjustable constant whose value of 0.65 is recommended for homogeneous turbulence by Shur et al. (1999). The model functions as a RANS model where $\tilde{d} = d$, and works as a subgrid-scale model where $\tilde{d} = C_{\text{DES}} \Delta$. Therefore, the behavior of the model is controlled by grid spacing.

The RANS region in DES alleviates the near-wall resolution requirement. Therefore, DES enables simulation of massively separated flows at high Reynolds numbers with a manageable computational cost.

2.2 Angle Definition

The definitions of yaw angle, inclination angle, and effective yaw angle used in this study are shown in Fig. 1. The yaw angle β is defined herein as the angle between the projection of the cylinder axis onto the horizontal plane (line CD) and a horizontal axis normal to the incoming flow (line CE). The inclination angle θ is defined as the angle between the cylinder axis (line AC) and its projection onto the horizontal plane (line CD). The effective yaw angle β^* is the angle between the cylinder axis (line AC) and its projection onto a plane normal to the incoming flow (line AB).

The angle of attack and local axes of the cylinder cross-section are also defined in Fig 1. The angle of attack γ is a local angle between the projection of the flow direction onto the plane of the cross-section (line OS) and the horizontal axis (line OP). The vertical axis is the “in-plane” direction, which is normal to the cylinder axis and is in the plane of points A, D, and C. The

horizontal axis is the “out-of-plane” direction which is normal to both the cylinder axis and the vertical axis. Local coordinates are defined on the basis of the cylinder axis and the flow direction. The local z axis is along the cylinder axis. The local x axis is on line OS and is perpendicular to the local y axis on the cross-section. Further details of the angles and local coordinates are given in Yeo and Jones (2008b).

2.3 Numerical Methods

Three-dimensional DES with the S-A DES model was conducted for a flow around a yawed and inclined circular cylinder at $Re = 1.4 \times 10^5$ (based on freestream velocity U and the diameter of the cylinder D). Cylinders of different spanwise aspect ratios ($L/D = 10, 20,$ and 30) were employed. The computational domain had an extent of $40D$ in the streamwise direction ($20D$ each in the upstream and downstream region), $40D$ in the cross-stream direction ($20D$ from the center of the cylinder to the top and bottom side), and a cylinder length of $10D, 20D$ and $30D$ in the spanwise direction.

The simulation employed a constant velocity for the upstream boundary, zeroth order extrapolation with fixed static pressure for the downstream boundary, and slip wall conditions for the top and bottom boundaries. To investigate the effect of spanwise wall boundary conditions on the flow structures, simulations with periodic and slip (or inviscid) conditions on spanwise wall boundaries were conducted as indicated in Fig. 2. Since the first grid normal to the cylinder surface was located around wall unit $y^+ = 1$ (this non-dimensional viscous length scale is based on the viscosity and wall shear stress of a flow), a no-slip condition on the surface was employed without wall treatments. The spanwise grid spacing in the local z axis was $0.167D$. Along the perimeter of the cylinder surface 128 grids were employed. The total size of the

computational grid was about 1.5×10^6 elements for the $10D$ case, 3.0×10^6 for $20D$, and 4.5×10^6 for $30D$. The numerical scheme used a fifth order upwind scheme for convection, a second order central scheme for viscosity, and a two-step MacCormack implicit scheme for time integration with four Newton sub-iterations per timestep. A non-dimensional timestep of $\Delta t^* = 0.01$ (calculated as $t^* = Ut/D$) was used.

The simulation assumed turbulent separation from the cylinder surface caused by the turbulent boundary layer flow on the surface before separation. This feature results from the inherent characteristics of DES: the upstream flow in DES has turbulent viscosity, which leads to the delay of flow separation from the cylinder. The characteristics of flow-induced pressures and forces in this study are in good agreement with those of turbulent flow at sub-critical Reynolds number and smooth flow at critical Reynolds number (Yeo, 2008).

For verification and validation of this simulation, the research conducted 1) 2-D and 3-D simulations of flows normal to a cylinder and 2) 3-D simulations of flows oblique to a cylinder. The verification process enabled to estimate and reduce the modeling errors due to numerical parameters: grid refinement, timestep, sub-iteration per timestep in the iteration method, order of schemes for convective terms. The validation process made it possible to assess the simulated results in comparison to experimental data and to identify the flow characteristics in the simulations. Further details are provided in Yeo and Jones (2011).

3. RESULTS OF SIMULATIONS

3.1 Vortex Flow Structures

Fig.3 shows vortex flow structures around the cylinders using an iso-surface of the second invariant Q of velocity gradient tensor $u_{i,j}$ (Hunt et al., 1988):

$$Q = \frac{1}{2}(\Omega_{ij}\Omega_{ij} - S_{ij}S_{ij}) = -\frac{1}{2}u_{i,j}u_{j,i} \quad (3)$$

where $\Omega_{ij} = \frac{1}{2}(u_{i,j} - u_{j,i})$ and $S_{ij} = \frac{1}{2}(u_{i,j} + u_{j,i})$ are the rotation rate and the strain rate, respectively. The invariant Q describes the balance between pure strain and fluid rotation. The surface of positive Q represents the region where the rotation overcomes strain in strength. It identifies coherent vortex structures effectively. The Q value of an iso-surface in Fig. 3 is 5000 [s⁻²] and the contour range of its color is from -300 to 300 [s⁻¹] in the vorticity of the local z axis along the cylinder.

In the case of periodic boundary conditions (Fig. 3(a) for a cylinder¹ of $L/D = 20$), vortex flow structures had inherent features of three-dimensional flow due to the relative angle between the cylinder axis and the flow direction, regardless of the aspect ratio. Flow structures with strong vorticity were observed around the cylinder. The vortex lines were not straight, nor linearly oblique to the cylinder axis. Shedding of the vortex flow was intermittently delayed around the cylinder where intense low pressure was generated. This phenomenon can be explained by the existence of swirling flows, which play an important role in generating intense low pressure on the local surface of the cylinder (Yeo and Jones, 2008b).

In the cases of slip boundary conditions (Fig. 3(b, c, d)), the vortex flow structures around all cylinders were significantly influenced over the entire lengths of the cylinders by the slip boundary condition. The flow was highly disturbed around the upper/upstream end of the cylinder compared to that around its lower/downstream end. The end effects from the upper/upstream end on the flow field persisted far behind the cylinder.

¹ A cylinder of an aspect ratio will be expressed hereafter in terms of the diameter.

For the 10D cylinder ($L/D = 10$; Fig. 3(b)), vortex flows were completely influenced over the entire length of the cylinder by the boundary conditions. By comparison, for the 20D and 30D cylinders (Fig. 3(c, d)), the vortex flows developed over part of the cylinder (i.e., downward from the midpoint of the cylinder length) and shed in a similar manner to Kármán vortex-shedding of flow normal to a cylinder.

It is notable that the delayed shedding of the vortex due to the swirling flow, as shown in the flows with the periodic conditions (Fig. 3(a)), was not clearly observed in the flows with the slip conditions. For the 20D and 30D cylinders, the effects of the slip walls seemed to be reduced in the part of cylinder that was further downward from the upper/upstream end and was upward from the lower/downstream end. However, the aspect ratios of the cylinders were not sufficiently high to generate swirling flows. Consequently, the flows could not completely develop along the lengths of the cylinders between the slip walls, even in the 30D cylinder. This implies that a spanwise aspect ratio of a cylinder should be carefully selected, especially in wind tunnel experiments, in order to reliably model the flow oblique to a very slender cylinder.

3.2 Characteristics of Forces

This study investigated aerodynamic forces on the cylinder for the different spanwise wall boundary conditions and aspect ratios. Fig. 4 shows distributions of force coefficients in space and time for 20D cylinders. Non-dimensional time (t^*) and length (z/D) were used for the abscissa and the ordinate, respectively. The force coefficients (C_x and C_y) in the local x and y axes are defined as

$$C_x = \frac{F_x}{\frac{1}{2}\rho U^2 A}, \quad C_y = \frac{F_y}{\frac{1}{2}\rho U^2 A} \quad (4)$$

where F_x and F_y are forces on the cylinder in the x and y axes, ρ is the density of the air, and A is a projected area of the cylinder normal to the wind direction.

As shown in Fig. 4, the spanwise boundary conditions significantly affected forces on the cylinder. For the periodic conditions (Fig. 4(a, b)), forces demonstrated inherently three-dimensional features that were induced by the fully developed flow along the cylinder axis. The fluctuations of the forces were correlated not over the entire length but within a finite length of the cylinder, and their peaks moved along the cylinder axis. The moving force peaks are seen as a series of oblique strips in the figures. Their slopes with respect to time indicate the speed of the force peaks traversing the cylinder length and are approximately 90% of the velocity component along the cylinder axis ($U\sin\beta^*$) of the incoming flow. Further details are given in Yeo and Jones (2008b).

For the slip conditions (Fig. 4(c, d)), forces were strongly influenced by the boundary conditions. Notably, the forces had strong, low-frequency components around the upper/upstream end (where z/D is zero in the figures). This phenomenon was not generated by inherent characteristics of the flow oblique to a cylinder, but rather was developed by the disturbance of the flow due to the slip conditions. However, although they were also influenced by the slip condition, no noticeable low-frequency component of forces was observed near the lower/downstream end, regardless of the aspect ratio. As the aspect ratio increased, the relative length influenced by the slip boundaries decreased, but the forces were not fully recovered from the influence of the slip spanwise boundary condition.

Fig. 5 shows time-averages and standard deviations of forces (C_x and C_y) along relative cylinder lengths under the slip boundary conditions. While forces on all the cylinders ($10D$, $20D$, and $30D$) had high average and fluctuating values near their upper/upstream ends (between $z/D =$

0 and $z/D \approx 10$), they had low average and fluctuating values within a distance of about $z/D \approx 5$ from their lower/downstream ends (e.g., between $z/D \approx 15D$ and $z/D = 20D$ for the $20D$ cylinder). This observation supports the assertion that the flow and the resulting forces are significantly affected by the boundary conditions.

To shed further light on the development of forces along the length of a cylinder oblique to flow between slip walls, the forces were compared with those on a cylinder between periodic walls for $30D$ cylinders. Details of force coefficients under periodic boundary conditions are given in Yeo and Jones (2008b). Fig. 6 shows relative ratios of force coefficients for slip walls to those for periodic walls along the cylinder axis; the ratio of unity indicates perfect agreement between forces of both conditions.

As shown in the figure, averaged C_x for slip walls is higher near the upper/upstream end and lower near the lower/downstream end than that for periodic walls, but the values for both conditions are in good agreement (i.e., close to unity) between $z/D \approx 7$ and $z/D \approx 26$. Averaged C_y for slip walls significantly fluctuates near the upper/upstream end and increases near the lower/downstream end; it is generally higher over the cylinder length than that for the periodic walls. Results confirm that averaged forces on a cylinder between slip walls are much influenced near ends by the end effect. The figure also shows that fluctuations of C_x and C_y for slip walls are reduced except at both ends for the slip condition. This means that the flow cannot be fully developed along a finite length of $30D$ between slip walls. The figure shows that the ratios of all forces are close to unity at a position of $z/D \approx 25$ on the $30D$ cylinder. However, because this feature was also observed at $z/D \approx 15$ on the $20D$ cylinder in Fig. 5, it suggests that the phenomenon is also caused by the end effects. Therefore, the forces generated using the slip conditions could not avoid the end effects at any position of the $30D$ cylinder.

Spectral characteristics of the forces were analyzed by fast Fourier transform (FFT) and were summarized in Table 1. Fig. 7 shows their spatial distributions along the cylinder lengths using the power spectral density (PSD) of force coefficients for both boundary conditions. The non-dimensional reduced frequency is defined as $f_r = Df/U$ where f is the oscillating frequency associated with the force.

For the periodic conditions, frequency components of the forces were distributed consistently over entire length of the cylinder. For the $20D$ cylinder (Fig. 7(a, b)), a dominant reduced frequency of C_x is 0.033. Two peak reduced frequencies of C_y are 0.165 and 0.198, which are 5 and 6 times as high as those associated with C_x . The difference between two peak reduced frequencies in C_y is consistent with the peak reduced frequency in C_x . C_y behaves as if it is generated by a beat phenomenon in which the amplitude reaches a maximum at a low frequency generated from the difference between two close, high frequencies. However, this modulating amplitude of C_y results from multiple moving forces at intervals that are induced by swirling flows. Further details on the flow were given in Yeo and Jones (2008b).

For the slip conditions, frequency components of the forces were quite differently distributed according to locations and aspect ratios of a cylinder. In the $10D$ cylinder (Fig. 7(c, d)), peak reduced frequencies of C_x and C_y are both $f_r = 0.048$ near the upper/upstream end. They are related to strongly disturbed flow due to the end effect. No noticeable component of low-frequency variation was observed around the lower/downstream end.

In the $20D$ and $30D$ cylinders (Fig. 7(e, f) and Fig. (g, h), respectively), C_x and C_y also have a peak low reduced frequency near the upper/upstream ends; both axes have $f_r = 0.054$ for $20D$ and $f_r = 0.040$ for $30D$. In contrast to forces on the $10D$ cylinder, the forces on both longer cylinders have a low reduced frequency in the x axis direction and relatively high reduced

frequencies in the y axis direction downward along the cylinder; forces on the $20D$ and $30D$ cylinders have $f_r = 0.020$ and 0.018 in the x axis (though they are not clearly seen in Fig. 7) and $f_r = 0.262$ and 0.135 in the y axis at $z/D \approx 15$ and 25 , respectively. These features have a trend similar to those of forces with the periodic condition (i.e., the low frequency in C_x and the high frequencies in C_y). However, it is noteworthy that dominant frequency components of the forces for the slip conditions are located around $\Delta z/D = 5$ upward from the lower/downstream ends where the maximum force fluctuation due to the end effects occurred (Fig. 6). Therefore, the results support the contention that an aspect ratio of 30 is not sufficiently high for flow to develop inherent three-dimensional features along a yawed and inclined circular cylinder between slip walls.

3.3 Suggestions for Wind Tunnel Tests

The present study approximated the required aspect ratio of a cylinder for full development of flow and the associated forces using results of simulations with the periodic boundary conditions. For flow simulation of a cylinder with the 30° yaw and 45° inclination angles used in this study, a non-dimensional time of $t^* \approx 100$ was required from the beginning of the simulation for flow to develop completely along the cylinder axis. As shown Fig. 4(a, b), the moving speed of a series of the flow-induced forces along the spanwise axis was estimated from the slope (i.e., speed) of the force peaks with respect to time. Thus, it was possible to estimate the location where the flow started to develop fully from the upper/upstream end as $z/D \approx 32$, using the calculated speed and the required time duration. Under the assumption that the same length is needed downward to avoid the effect of the lower/downstream end, the cylinder requires a minimum aspect ratio of 64 between slip walls to simulate flow around the yawed and inclined

cylinder of infinite extent. This estimate cannot be applied directly in the design of a model for experiments until all conditions of the test are taken into account. However, it is noted that the required spanwise aspect ratio ($L/D \approx 64$) estimated in this study is much longer than those used in most experiments: for example, $L/D = 24$ by Matsumoto et al. (2007) and $L/D = 27$ by Cheng et al. (2008).

This study also suggested appropriate positions of pressure-measuring devices, such as pressure taps, on the cylinder surface where flow structures are most developed along the cylinder length in three dimensions. For effective pressure measurement to mitigate the end effects, pressure taps should be located approximately from one half to two-thirds of the cylinder length from its upper/upstream end under the assumption that the slenderness of the cylinder is in compliance with the requisite spanwise aspect ratio.

4. CONCLUSIONS

Detached eddy simulations in three dimensions were conducted on flow oblique to a circular cylinder at $Re = 1.4 \times 10^5$. Different spanwise aspect ratios ($L/D = 10, 20, \text{ and } 30$) and spanwise boundary conditions (periodic and slip) were employed to investigate how the length of an oblique cylinder affects development of flow around the cylinder and the associated forces on it.

Results showed that both boundary conditions and spanwise aspect ratio significantly affect flow oblique to a cylinder. Simulations with periodic spanwise boundary conditions showed that flow around the cylinder fully developed along the spanwise axis in three dimensions, irrespective of the aspect ratio investigated in the study. Alternately developing swirling flows generated multiple force peaks that moved along the cylinder. This mechanism of force generation can excite the cylinder at a much lower frequency than classical Kármán vortex-

induced forces. In contrast, simulations with slip spanwise boundary conditions showed no fully developed flow along the spanwise axis for any of the three aspect ratios examined in this study. A $10D$ cylinder showed disturbed flow over the entire length attributable to the end effects. Even in a $30D$ cylinder, the flow and the resulting forces did not fully develop along the cylinder axis. In particular, the flow around the upper/upstream end of the cylinder generated low-frequency forces on the corresponding part of the cylinder. The low frequency of the forces was not related to the inherent characteristics of forces due to flow oblique to a cylinder, but rather resulted purely from the end effect.

The significant end effect of slip conditions indicates that the end effect interferes with development of flow along the cylinder. This is of critical importance because this study showed that the aspect ratio of a cylinder plays a crucial role in developing inherent three-dimensional flow completely along the spanwise axis. To simulate inherent characteristics of flow-induced forces along a very slender cylinder, the flow and the associated forces must fully develop. Therefore, an implication of this numerical study for experimental investigations is that studies on flow oblique to a slender cylinder should ensure that a cylinder has a sufficiently high aspect ratio to develop inherent characteristics of flow developing along its axis.

The requisite cylinder aspect ratio for flow development estimated in this study would be approximately 60 for the case of the 30° yaw and 45° inclined cylinder, which is much higher than what has been employed in wind tunnel tests. For effective measurement of the flow-induced pressures, pressure taps are suggested to be located from a half to two-thirds of the cylinder length from its upper/upstream end when the slenderness of the cylinder is satisfied with the requisite spanwise aspect ratio. In order to reliably predict the required aspect ratio and appropriate pressure-measuring positions of a cylinder for full development of flow in wind

tunnel tests, however, numerical simulations would require modeling of boundary-layer flow near the side walls and modeling of blunt ends of the cylinder and end plates (if used). Such numerical results would provide to experimentalists more specific information on reliable measurements that are least influenced by inherent end effects due to their test conditions.

REFERENCES

- Cheng, S., Larose, G.L., Savage, M.G., Tanaka, H., Irwin, P.A., 2008. Experimental study on the wind-induced vibration of a dry inclined cable - Part I: Phenomena. *Journal of Wind Engineering and Industrial Aerodynamics* 96(12), 2231-2253.
- Hikami, Y., Shiraishi, N., 1988. Rain-wind induced vibrations of cables stayed bridges. *Journal of Wind Engineering and Industrial Aerodynamics* 29(1-3), 409-418.
- Hunt, J.C.R., Wray, A.A., Moin, P., 1988. Eddies, stream, and convergence zones in turbulent flows. Report CTR-S88, Center for Turbulence Research.
- Kawamura, T., Hayashi, T., 1994. Computation of flow around a yawed circular cylinder. *JSME International Journal Series B* 37(2), 229-236.
- Kohama, Y., Motegi, D., 1994. Traveling disturbance appearing in boundary-layer-transition in a yawed cylinder. *Experimental Thermal and Fluid Science* 8(4), 273-278.
- Larose, G.L., Savage, M.G., Jakobsen, J.B., 2003. Wind tunnel experiments on an inclined and yawed circular cylinder in the critical Reynolds number range, in: *Proceedings of the 11th International Conference on Wind Engineering*, Lubbock, Texas, 1705-1712.
- Lucor, D., Karniadakis, G., 2003. Effects of oblique inflow in vortex-induced vibrations. *Flow, Turbulence and Combustion* 71(1-4), 375-389.
- Matsumoto, M., Daito, Y., Kanamura, T., Shigemura, Y., Sakuma, S., Ishizaki, H., 1998. Wind-induced vibration of cables of cable-stayed bridges. *Journal of Wind Engineering and Industrial Aerodynamics* 74-76, 1015-1027.
- Matsumoto, M., Shiraishi, N., Kitazawa, M., Knisely, C., Shirato, H., Kim, Y., Tsujii, M., 1990. Aerodynamic behavior of inclined circular cylinders-cable aerodynamics. *Journal of Wind Engineering and Industrial Aerodynamics* 33(1-2), 63-72.
- Matsumoto, M., Yagi, T., Adachi, Y., Hatsuda, H., 2007. Karman vortex effects on aerodynamic instabilities of inclined stay-cables, in: *Proceedings of the Twelfth International Conference on Wind Engineering*, Cairns, Australia, 175-182.
- Matsumoto, M., Yagi, T., Liu, Q., Oishi, T., Adachi, Y., 2005. Effects of axial flow and Karman vortex interferences on dry-state galloping of inclined stay-cables, in: *Proceedings of the Sixth International Symposium on Cable Dynamics*, Charleston, SC.
- Matsuzaki, K., Shingai, M., Haramoto, Y., Munekata, M., Ohba, H., 1994. Visualization of three-dimensional flow structures in the wake of an inclined circular cylinder. *Journal of Visualization* 7(4), 309-316.
- Phelan, R.S., Sarkar, P.P., Mehta, K.C., 2006. Full-scale measurements to investigate rain-wind induced cable-stay vibration and its mitigation. *Journal of Bridge Engineering* 11(3), 293-304.
- Ramberg, S.E., 1983. The effects of yaw and finite length upon the vortex wakes of stationary and vibrating circular cylinders. *Journal of Fluid Mechanics* 128(1), 81-107.
- Shirakashi, M., Hasegawa, A., Wakiya, S., 1986. Effect of the secondary flow on Karman vortex shedding from a yawed cylinder. *Bulletin of the JSME-Japan Society of Mechanical Engineers* 29(250), 1124-1128.
- Shur, M.L., Spalart, P.R., Strelets, M., Travin, A., 1999. Detached-eddy simulation of an airfoil at high angle of attack, in: *Proceedings of the 4th International Symposium on Engineering Turbulence Modelling and Measurements*, Corsica, 676-682.

- Spalart, P.R., Allmaras, S.R., 1992. A one-equation turbulence model for aerodynamic flows, in: Proceedings of the 30th Aerospace Sciences Meeting and Exhibit, Reno, NV, 1-22.
- Spalart, P.R., Jou, W.H., Strelets, M., Allmaras, S.R., 1997. Comments on the feasibility of LES for wings, and on a hybrid RANS/LES approach, in: Proceedings of the Advances in DNS/LES, 1st AFOSR International Conference on DNS/LES, Ruston, LA, 137-147.
- Tournier, C., Py, B., 1978. The behavior of naturally oscillating three dimensional flow around a cylinder. *Journal of Fluid Mechanics* 85, 161-186.
- Yeo, D., 2008. Numerical simulation of 3-D aerodynamic behavior of a yawed, inclined circular cylinder. Ph.D. thesis, University of Illinois at Urbana-Champaign, Urbana.
- Yeo, D., Jones, N.P., 2006. Numerical simulation of unsteady 3-D flow around a yawed and inclined circular cylinder, in: Proceedings of the 4th International Symposium on Computational Wind Engineering, Yokohama, Japan, 455-458.
- Yeo, D., Jones, N.P., 2008a. Effects of spanwise boundary conditions and aspect ratios on flow around a yawed and inclined circular cylinder, in: Proceedings of the 4th International Conference on Wind and Structures, Jeju, Korea, 1693-1705.
- Yeo, D., Jones, N.P., 2008b. Investigation on 3-D characteristics of flow around a yawed and inclined circular cylinder. *Journal of Wind Engineering and Industrial Aerodynamics* 96(10-11), 1947-1960.
- Yeo, D., Jones, N.P., 2011. Computational Study on 3-D Aerodynamic Characteristics of a Yawed, Inclined, Circular Cylinder. No. NSEL-027, University of Illinois at Urbana-Champaign, Urbana, IL.
- Zuo, D., 2005. Understanding wind- and rain-wind induced stay cable vibrations. Ph.D. thesis, the Johns Hopkins University, Baltimore.
- Zuo, D., Jones, N.P., 2006. Understanding wind- and rain-wind-induced stay cable vibrations from field observations and wind tunnel tests, in: Proceedings of the 4th U.S.-Japan Workshop on Wind Engineering, Tsukuba, Japan.

List of Tables

Table 1. Peak reduced frequencies of aerodynamic forces..... 22

Table 1. Peak reduced frequencies of aerodynamic forces

B.C.	L/D	Upper/upstream end		Lower/downstream end	
		$f_r(C_x)$	$f_r(C_y)$	$f_r(C_x)$	$f_r(C_y)$
Periodic wall	20	0.033	0.165	0.033	0.165
	10	0.048	0.048	-	-
Slip wall	20	0.054	0.054	0.020	0.262
	30	0.040	0.040	0.018	0.135

List of Figures

Fig. 1 Definition of angles	25
Fig. 2 Computational domain ($L/D = 30$)	26
Fig. 3 Vortex flow structures of $Q = 5,000 \text{ [s}^{-2}\text{]}$	27
Fig. 4 Spatial and temporal distribution of aerodynamic force coefficients ($L/D = 20$).....	28
Fig. 5 Characteristics of aerodynamic forces along cylinder lengths	29
Fig. 6 Ratios of aerodynamic force coefficients along cylinder length ($L/D = 30$)	30
Fig. 7 Spatial distribution of frequency of forces	31

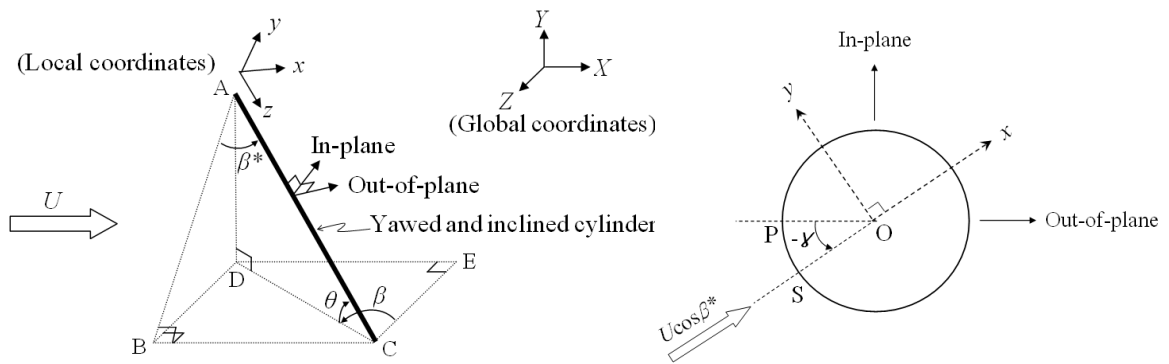


Fig. 1 Definition of angles

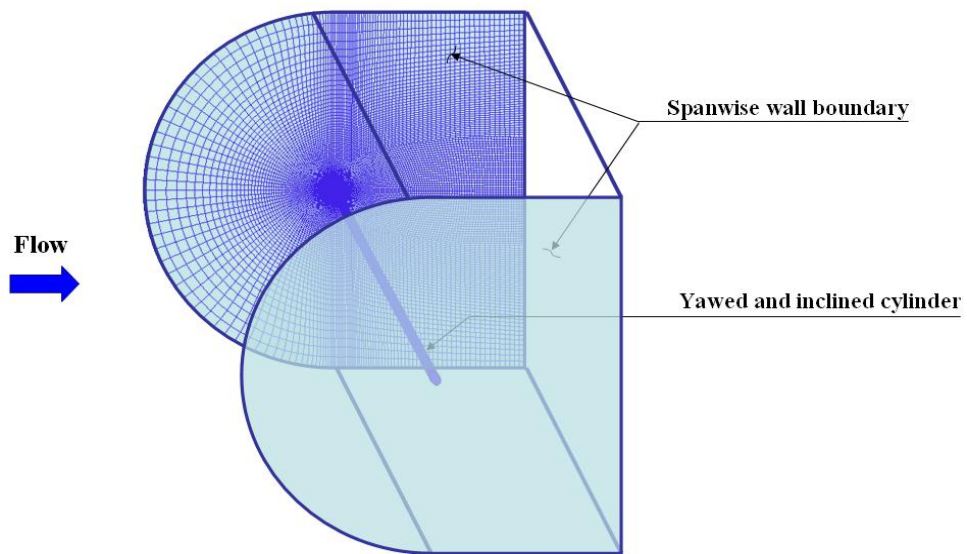
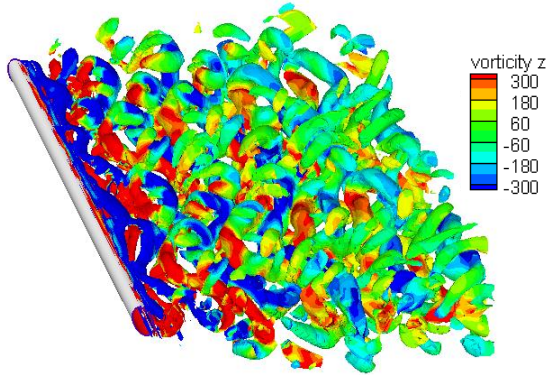
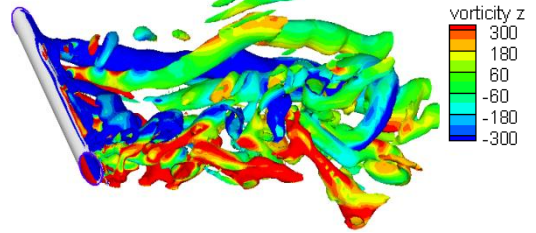


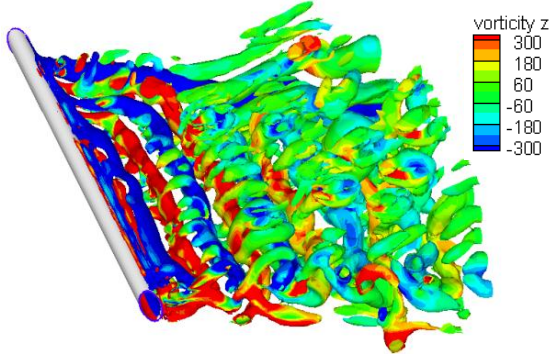
Fig. 2 Computational domain ($L/D = 30$)



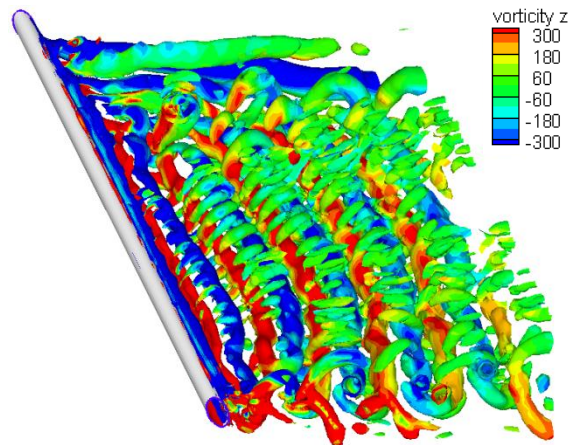
(a) Periodic wall ($L/D = 20$)



(b) Slip wall ($L/D = 10$)

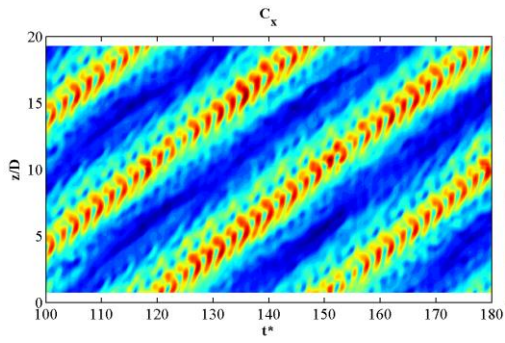


(c) Slip wall ($L/D = 20$)

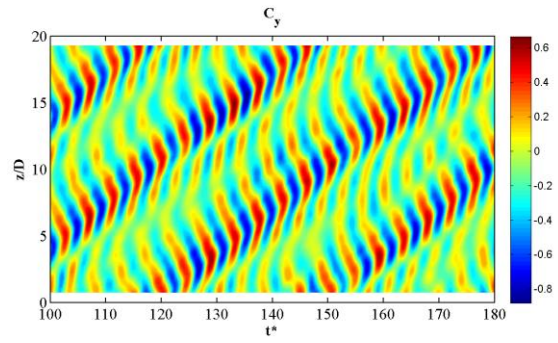


(d) Slip wall ($L/D = 30$)

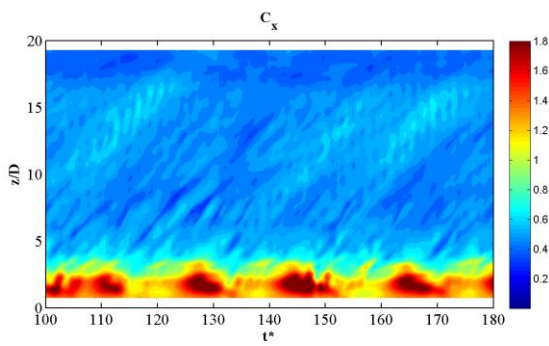
Fig. 3 Vortex flow structures for $Q = 5,000 \text{ [s}^{-2}\text{]}$



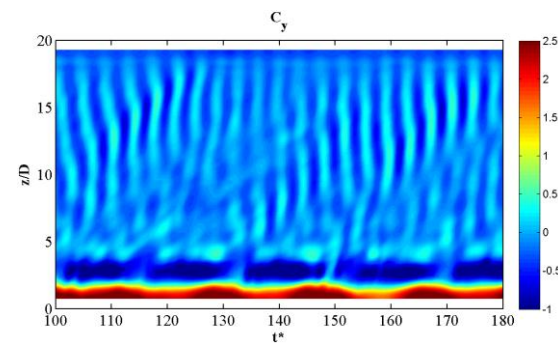
(a) C_x (periodic wall)



(b) C_y (periodic wall)

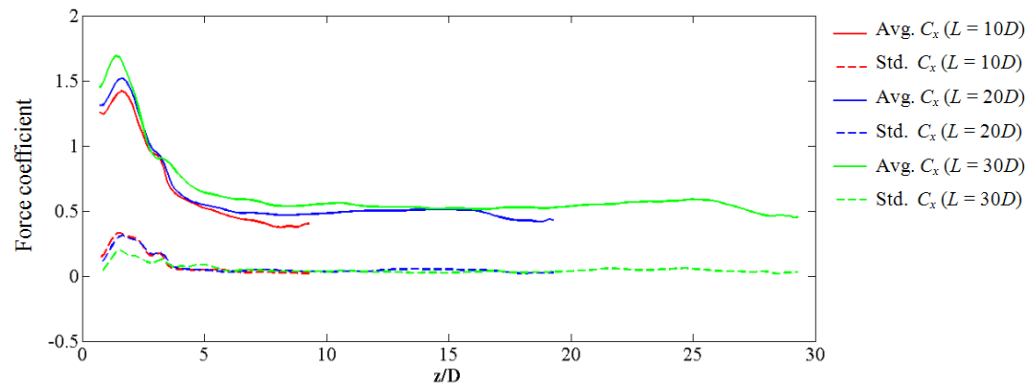


(c) C_x (slip wall)

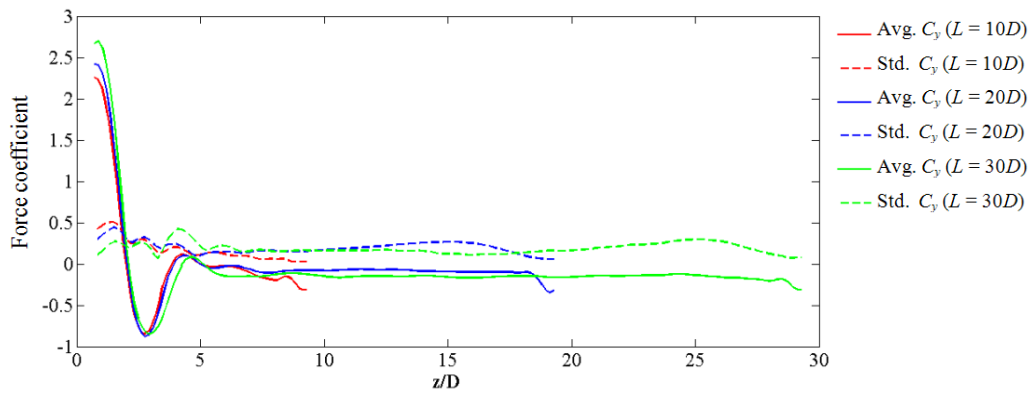


(d) C_y (slip wall)

Fig. 4 Spatial and temporal distribution of aerodynamic force coefficients ($L/D = 20$)



(a) C_x



(b) C_y

Fig. 5 Characteristics of aerodynamic forces along cylinder lengths

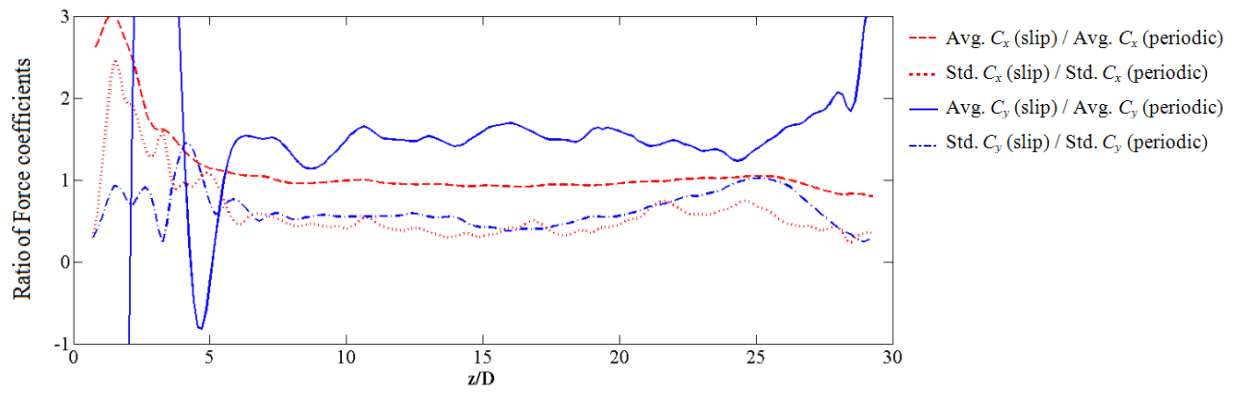


Fig. 6 Ratios of aerodynamic force coefficients along cylinder length ($L/D = 30$)

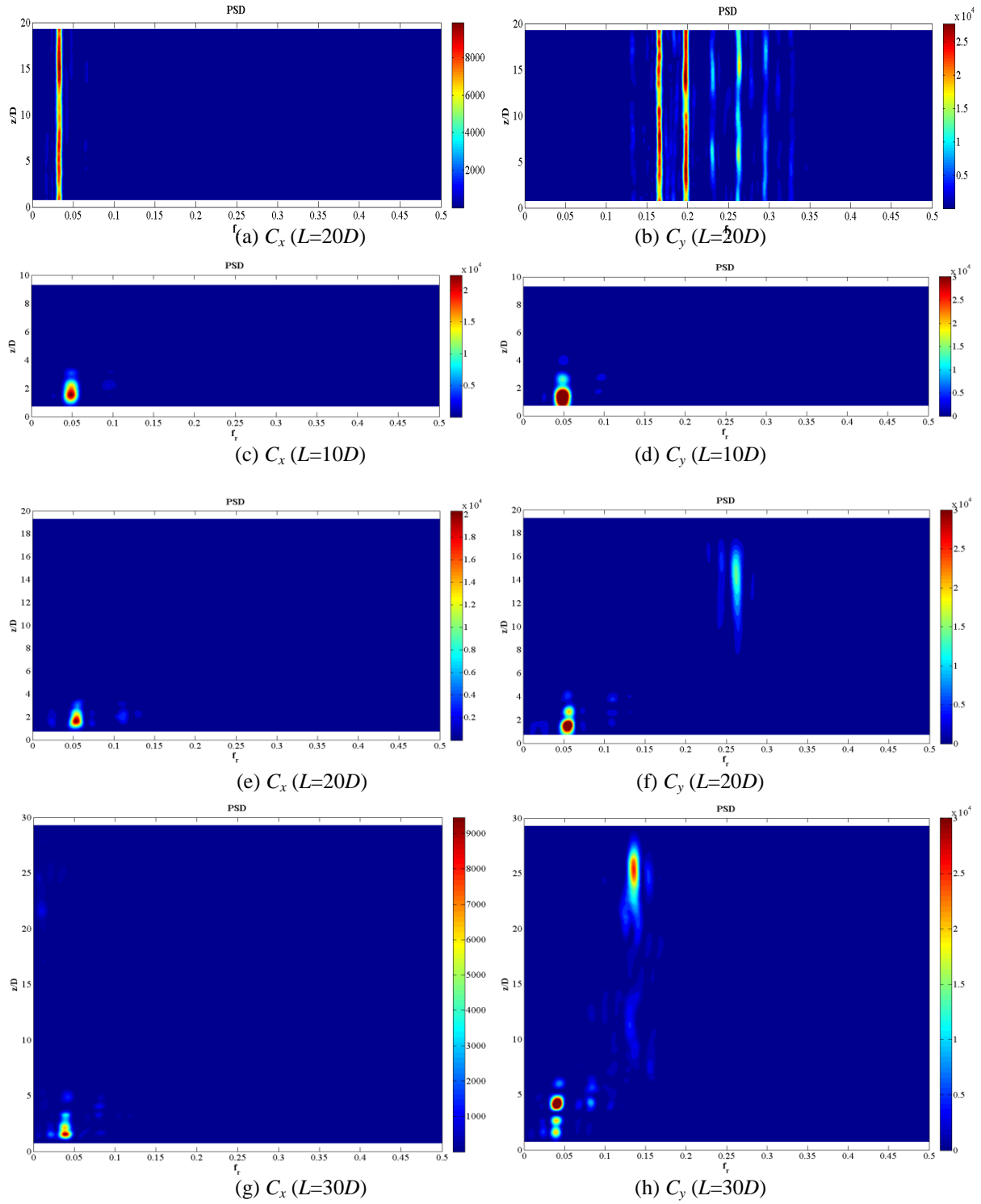


Fig. 7 Spatial distribution of frequency of forces ((a) and (b) for periodic B.C.; (c) to (h) for slip B.C.)